ADVANCED ENGINEERING MATERIALS
www.aem-journal.com

A Real-Time Process Diagnostic to Support Reliability, Control, and Fundamental Understanding in Aerosol Jet Printing

*Jeremy D. Rurup and Ethan B. Secor**

Aerosol jet printing is a compelling technology for hybrid electronics, combining digital and noncontact patterning with broad materials compatibility, resolution as fine as ≈10 microns, and a high standoff distance of 1–5 mm. Despite its growing popularity in research environments, a robust process understanding and improved manufacturing control are essential for achieving the reliability and predictability required for broader adoption in advanced applications. Herein, recent developments in process monitoring using in-line light scattering measurements are discussed, including their mechanistic foundations, experimental validation, relevance for process control and reliability, and value as a diagnostic tool for fundamental studies. Experimental measurements confirm the correlation between measured light scattering and deposition rate. Building on this platform, feedback from the real-time measurement is coupled with printer software to support automated closed-loop control via a simple proportional-integral-derivative software control loop. Combined with the utility of these measurements as a diagnostic to accelerate ink formulation and support fundamental process science experiments, this in-line measurement provides a useful tool to improve print reliability with the potential to advance the adoption and capabilities of this method in conformal, flexible, and hybrid electronics applications.

1. Introduction

Aerosol jet printing (AJP) is a promising candidate for advanced manufacturing of electronic devices and systems.[1] AJP is a digital, additive technology supporting noncontact deposition of functional liquid inks with resolution approaching 10 microns.[2] The suitability of this method for multilayer patterning of conductive, dielectric, and semiconducting materials,[1] its 1–5 mm nozzle-surface standoff distance for conformal printing on nonplanar surfaces,[3] and advantages of digital patterning for rapid prototyping and small volume production provide compelling characteristics for a wide range of applications. A small subset from the recent literature spans advanced electronics packaging,[4–7] biomaterials,[8,9] conformal patterning,[10,11] catalysis,[12] and a wide range of sensors.[13–15]

Despite its promise, the broader adoption of AJP in production environments remains hindered by several challenges. In particular, the manufacturing tolerances and quality control requirements typical of commercial applications and well-controlled experiments remain a key challenge for AJP, which exhibits inherent variability and drift that is difficult to control or compensate.[16,17] The serial nature of AJP further demands part-specific qualification for high-value applications, as stochastic processes introducing defects could affect isolated prints. Sparse sampling for quality control, typical of highly parallel manufacturing, provides only limited confidence for this serial production framework.

Several approaches have been introduced in recent years to address the important challenge of AJP process reliability. Salary and Poliks et al. developed an online imaging system to evaluate print characteristics in place, allowing quick feedback to users based on metrology of printed lines.[18] More recent efforts from this group have included image-based control using active monitoring of the printed line width, using both classical control and machine learning.[19,20] Hines, et al. moved one step upstream in the process, timing the filling of microfabricated inkwells to directly calculate a wet deposition rate of the ink.[21] A third strategy, moving one step further upstream and constituting the focus of this work, uses an optical scattering measurement upstream of the printhead to provide a real-time measurement correlated with the deposition rate.[22] This evolution toward upstream detection results in a tradeoff: the measurement provides a less direct diagnostic of printing observables (i.e., resolution and thickness), but is readily connected to fundamental process mechanisms.

Here, we focus broadly on this physics-based approach to AJP process monitoring. We first provide a summary and explanation of capabilities demonstrated to date, including the underlying physical model and assumptions associated with this method. This starts with an understanding of dominant sources of drift,

J. D. Rurup, E. B. Secor
Department of Mechanical Engineering
Iowa State University
Ames, Iowa 50011, USA
E-mail: esecor@iastate.edu

DOI: 10.1002/adem.202301348

motivating the development of an in-line measurement system that operates during printing to detect process variability. With this foundation, the real-time measurement can support three valuable functions: 1) offering a real-time, quantitative input for a feedback control framework to mitigate long-term drift in fabrication output; 2) establishing process data that predicts functional properties of the printed device and can support digital quality monitoring; and 3) providing a quantitative in-line diagnostic to guide process development and support more sophisticated and fundamental mechanistic studies. While the basic elements of this technology have been described previously,[22–24] this Perspective article serves to provide a holistic primer on the foundations of this technology, a critical assessment of its opportunities and limitations, and an introduction to the nascent implementation of this technology for fundamental process diagnostics.

2. Foundations

While there can be many potential sources of variability during AJP, we focus on the most intractable, effectively assuming that best practices to control ink composition, temperature, and environmental conditions are adopted. Even with all these elements well controlled, it has been shown that changes to the amount of ink in the cartridge–a typical outcome of printing–can induce changes in atomization.[17] While this was experimentally shown for AJP using ultrasonic atomization (UA), it is expected that the even more complex pneumatic atomization (PA) mechanism is also sensitive to this, as it will influence the hydraulic pressure on the ink within the atomization nozzle and affect recirculation of ink within the cartridge. While a recirculating cartridge has been shown to limit very long-term drift,[17] and a split stream solvent add back offers a clever approach to mitigate composition drift for PA,[25] this still leaves short term, stochastic changes in atomization or aerosol transport through the mist tubes as sources of variability. Optimized inks and printing conditions have been studied for long-duration fabrication runs with only limited drift,[26] but the manual effort to create such process recipes, and their limited scope across inks and materials, is an impediment to broader adoption of AJP.

The direct outcome of changes to aerosol generation and transport is a change in the deposition rate of material.[27] This can have secondary effects on the line resolution, overspray profile, and microstructure due to the complex physical mechanisms within the printhead and on the substrate coupling evaporation, aerodynamic effects, fluid dynamics, and ink chemistry.[28,29] While the flow field of the gas is certainly relevant for these effects, its highly controlled nature under standard conditions eliminates it from consideration as a root source of process drift under optimal operation. The process monitoring and control framework discussed here thus focuses principally on the deposition rate as an indicator of drift in generation and transport of aerosol droplets.

To describe the deposition rate based on physically relevant process parameters, the volume flow rate of ink traveling through the mist tube can be described by $f_a \nu_a$, with f_a the carrier gas flow rate (CGFR) and ν_a the volume fraction of aerosol droplets. To relate this to the volume flow rate of solid material, a multiplier of the solids volume fraction of the ink, χ_s, is included. To account for inefficiencies in impaction, an impaction efficiency term, η_i, is incorporated, giving an actual deposition rate (r_{dep}) of

$$r_{dep} = f_a \nu_a \chi_s \eta_i \tag{1}$$

Variability in the deposition rate, then, must be reflected in one or more of these parameters. The CGFR is controlled by a high precision (<1% accuracy) mass flow controller. The solids volume fraction of the ink can in principle change, particularly for dilute solutions and dispersions based on volatile solvents. However, process drift is observed even in carefully controlled experiments with constant composition, suggesting this is not in general the primary cause. The impaction efficiency under normal printing conditions is expected to be similar to unity, and is itself not a fundamental variable but a function of the aerosol volume fraction and gas flow field. This leaves the aerosol volume fraction as the key parameter, a conclusion validated by experiments.[22]

To develop a quantitative indicator of the aerosol volume fraction, this system exploits the strong Mie scattering of light characteristic of aerosol droplets in the size range typical to AJP (1–5 μm). In principle, the power of light scattered from the dilute aerosol stream (P_{sc}) depends on many parameters and can be approximated as

$$P_{sc} = P_0 \rho_N l \Omega \eta_o \sigma(d, \lambda, n, k, \theta, \varphi) \tag{2}$$

Here, P_0 is an incident power, ρ_N is the droplet number density, l is the path length, Ω is the collection solid angle, η_o is an efficiency describing the optical system components, and σ is the differential scattering cross section, which may be more formally denoted as $d\sigma/d\Omega$ and is itself a complex function of droplet diameter, light wavelength, optical constants of the droplet and continuous phase, and angles. Here, the droplet number density can be replaced by $\nu_a/\overline{V}_{drop}$, with $\overline{V}_{drop}$ an average droplet volume. Assuming a dilute aerosol and steady droplet size distribution and composition, the deposition rate is then proportional to the light scattering power as

$$r_{dep} \propto f_a \chi_s \eta_i \left(\frac{P_{sc}}{P_0} \frac{\overline{V}_{drop}}{l \Omega \sigma} \right) \tag{3}$$

In practice, the complexities of this equation can be readily accounted for by ink- and process-specific calibration and the polydisperse aerosol smooths variations in σ expected from Mie scattering theory. The wavelength of light influences the scattering nonlinearly, as Mie scattering is governed by the size parameter describing the droplet size relative to the light wavelength. With a polydisperse distribution of droplet sizes, and a single angle of scattering measured, this is effectively accounted for by calibration. Notably, effective process monitoring has been demonstrated with both broadband and narrowband light sources,[23,24] tolerating variations in optics system design to account for other considerations, such as availability and cost of light sources and detectors as long as stable light output is maintained.

This discussion of fundamentals is included here to emphasize that this method is based on AJP process physics, rather than a top-down systems engineering approach, and is thus generalizable and provides significant mechanistic insight as a process diagnostic. This derivation also highlights a key limitation of the single-measurement process monitoring strategy, in that a constant droplet size distribution is a necessary assumption. The

error that can be introduced by changes to the droplet size distribution has not yet been validated, but the experimentally observed linear correlation between deposition rate and scattering power provides support for this assumption. Alternative techniques for online AJP validation, based on volumetric filling of inkwells or image analysis, provide promising complementarity to this approach but without some benefits of its operando, digitally native nature.[18,21]

3. Results and Discussion

While the deposition rate is commonly considered as a dry volumetric deposition rate (volume of solid sample following postprocessing per unit time), to provide a more intuitive and versatile metric, we normalize the volumetric deposition rate to the printing speed. This speed-normalized, or linear, deposition rate is equivalent to the cross-section area of a single trace.[29] This is useful for designing patterns, as the number of passes required to reach a certain thickness can be easily calculated regardless of the pattern complexity, and it also makes explicit the significance of the printing speed. Moreover, it is this linear deposition rate–not primarily the volumetric deposition rate–that strongly affects the line resolution under a broad range of printing conditions, and thus stabilizing the linear deposition rate will offer some benefit for reducing variation in line width.[29]

The simplicity of the linear deposition rate as a key metric–namely, its correspondence to the cross-section area of a single trace–guides experimental design. Rather than printing a volumetric feature and profiling the full 3D surface to measure a deposited volume, or evaluating deposition rate by mass, which can be feasible for high solid-loading inks if short-duration granularity in output is not needed, a linear feature containing a fixed number of passes is printed and a cross-section area measurement via profilometry allows straightforward calculation of the linear deposition rate.

3.1. Proof of Concept

The necessary proof of concept to demonstrate the validity of optical scattering as a deposition rate indicator is a strong correlation between the actual linear deposition rate and the linear deposition metric (LDM), a composite parameter consisting of the CGFR, the scattering power, and the print speed as

$$LDM = \frac{f_a P_{sc}}{\nu_f} \tag{4}$$

with ν_f the printer feed rate or speed.[24] The nomenclature here is selected to imply the theoretical proportionality between the LDM and linear deposition rate. An optics cell was integrated with the printing system upstream of the junction between the carrier and sheath flows (**Figure 1**a), so that the interrogated

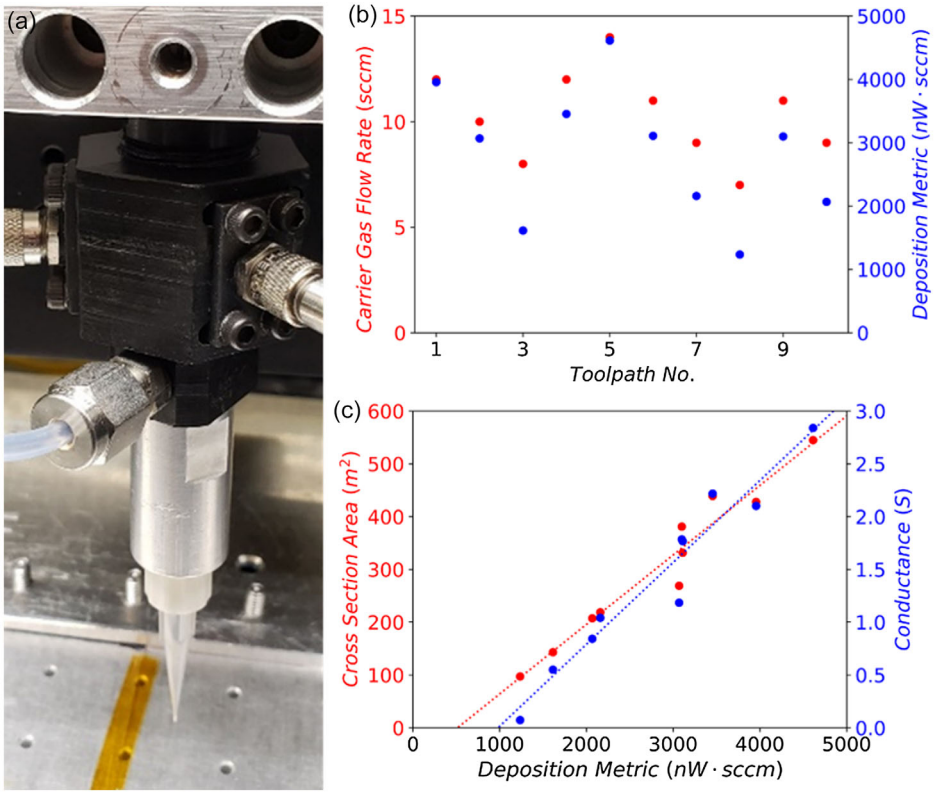

Figure 1. a) Photograph of an optics cell integrated with the aerosol jet printing system. b) Response of the deposition metric during an experiment in which the CGFR was varied. c) Confirmation of linearity between the deposition metric and both cross-section area and conductance for printed silver samples. Dashed lines indicate linear regression, with correlation coefficients of 0.95 and 0.94 for area and conductance, respectively.

aerosol is comprised entirely of the carrier gas mist. This optics cell contains two fiber-optic connectors, one for light input into the cell and one to guide scattered light to a photodetector. Importantly, the optics cell is entirely sealed other than the mist inlet and outlet, which are aligned in a vertical channel for the aerosol droplet flow. The light plane is perpendicular to this flow channel to simplify interpretation of the measurement.

As a proof of concept test, a silver nanoparticle (AgNP) ink was printed while varying the CGFR to fabricate bars, each containing 10 overlapping traces to build up reasonable thickness. Following printing and curing, both the cross-section area and resistance of 10 samples were measured. A simplified deposition metric–the product of scattering power and CGFR–is considered as a predictor for the deposition rate, neglecting the print speed effects in this narrow experiment because print speed is held constant. This is calculated based on the average scattering power during printing of each individual sample. As shown in Figure 1b, as the CGFR is adjusted for each sample, the deposition metric responds, but not in a completely proportional manner. As shown in Figure 1c, this deposition metric is a strong predictor of the actual cross-section area for each bar, with a correlation coefficient of 0.95. Because the conductance of a line is in principle proportional to its cross-sectional area (assuming constant conductivity), the deposition metric is also a strong indicator of sample conductance, here with a correlation coefficient of 0.94. While this is expected, it confirms only slight variation in resistivity across the ≈300% variation in deposition rate, and moreover illustrates the viability of the real-time deposition metric for predicting functional electrical properties.

3.2. Closed-Loop Control

Extending from processing monitoring–measuring the scattering power as an indicator of deposition rate in real time–to process control requires the identification and tuning of suitable control parameters. To date, atomizer voltage, CGFR, and print speed have been employed for closed-loop control demonstrations to maintain a constant speed-normalized deposition rate based on the LDM.[24] This functionality is demonstrated in **Figure 2**. During this test, the AgNP ink was printed over 90 min to fabricate 80 individual samples. During printing, the PID loop continuously calculated the LDM based on scattering measurements and adjusted the UA voltage to maintain a stable LDM output. As shown in Figure 2a, during the first 60 min of the test, little active control was required, and the UA voltage was stable within 0.5 V of 23 V. However, after 60 min, the scattering power began to decrease somewhat, bringing the LDM below the target value. In response, the automated controller began to increase the UA voltage, with a nonmonotonic change from ≈23 to ≈28.5 V between minute 60 and 90 to maintain stable aerosol generation, and thus consistent LDM.

Figure 2b shows the success of this automated control. Here, the LDM is averaged within each sample for the same dataset, and both time-averaged LDM and sample electrical resistance are overlaid. By maintaining a stable LDM, the resistance of samples remains consistent, demonstrating that the closed-loop controller can effectively extend the process duration beyond 60 min, where strong drift was beginning to occur. Some downward drift in resistance

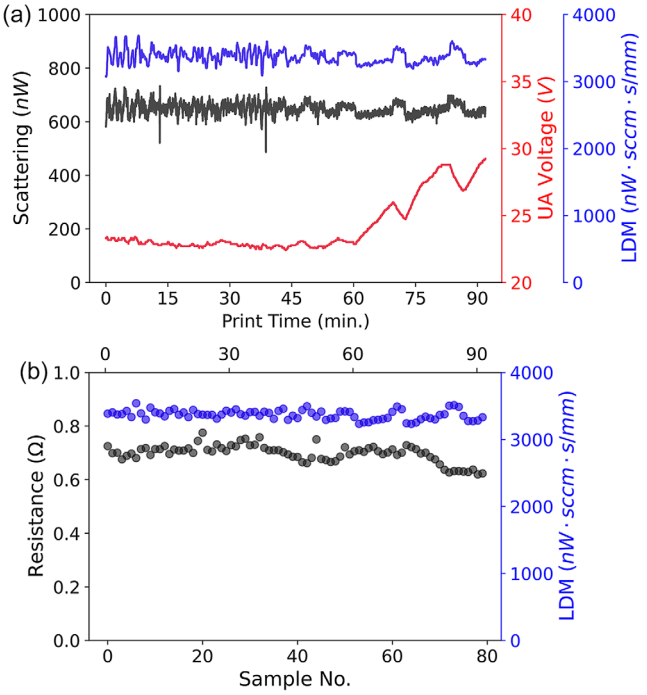

Figure 2. Demonstration of closed-loop control for AJP, including a) process data showing a response in the UA voltage to maintain stable LDM and b) correspondence between LDM and sample resistance over the 90-minute printing run.

is observed at the very end of the test, as the system moves further outside the calibrated range and secondary effects can play a role, such as changes to ink composition or droplet size distribution.

This shows that large changes to a process variable such as the UA voltage can lead to inaccuracy in the closed-loop control calibration. This could be compensated for with a more complex process model (i.e., including nonlinear effects and more variables) with more extensive calibration data. This digital method is also well aligned with data-driven tools for process control, which could provide more robust multifactor control but likely require more thorough calibration datasets. Even if variations in output cannot be effectively controlled outside of a narrow window, the real-time identification of drift mechanisms could allow more informed operator response. For this example, the UA voltage rising higher than 25–26 V could trigger an automatic production pause and alert an operator, so that necessary steps such as refilling the ink cartridge or cleaning and resetting the system could be implemented prior to continuing. Moreover, the benefit is more clear when considering the alternative of conventional open-loop operation. Using this same AgNP ink, a 37% increase in deposition rate is observed over 50 min of printing in a control experiment.[24] Representative of arbitrary inks for AJP more broadly, Smith et al. observed a nearly 4X increase in cross-section area over 60 min of printing.[16]

3.3. Process Quality Monitoring

While the process control framework is effective for mitigating long-term process drift (≈10's of minutes timescale), the slow

nature of any response parameter will necessarily limit its ability to respond to rapid (seconds timescale) fluctuations in deposition. This is because changes to the UA voltage and CGFR take time to fully propagate through the printing system–a response that can be quantified using this measurement system.

Thus, when short-term variation in printing does occur, the objective for the process monitoring system is to record that variation and correlate it spatially within the printed part, rather than compensating for it. A simple demonstration of this is shown in **Figure 3** for the AgNP ink. Here, a serpentine toolpath was printed onto glass, and random perturbations in printing were introduced manually. The colormap shows the simulated thickness over the x-y pattern of the toolpath using actual scattering data and nozzle positions during fabrication, with a low region evident in the serpentine region of the print. This is an initial exploration for the viability of this process monitoring framework to inform quality assurance of prints by providing a real-time metric during printing that can be spatially correlated with the physical geometry and ultimately with functional properties.

3.4. Process Diagnostic Utility

Because the optical measurement provides an indicator of the aerosol state within the printhead, it can be a useful diagnostic for guiding ink formulation and process development. While optimization of ink formulation and printing parameters is typically a time-consuming process, and therefore one done incompletely for most laboratory studies, the in-line measurement provides immediate feedback without any postprocessing and subsequent characterization. This can accelerate identification of printing protocols or allow more standardization in conditions. It can also provide key insight on physical mechanisms of the process that are difficult to obtain directly from characterization following printing.

Rurup et al. demonstrated this previously, using a PMMA ink and sweeping printing parameters to evaluate the response in light scattering.[24] For the sweep in the atomizer voltage, three different CGFR settings were used—12, 13, and 14 sccm. The change in the linear deposition metric reflects a change in the CGFR, along with a change in the aerosol volume fraction as indicated by the scattering power. As shown in **Figure 4** (top), the LDM exhibits a logistic response to the atomizer voltage, which is described by

$$LDM = \frac{LDM_{\mathrm{m}}}{1 + \exp\left[-C_{\mathrm{V}}(V_{\mathrm{atm}} - V_{\mathrm{thr}})\right]} \tag{5}$$

This type of response suggests a transition or "threshold" value (V_{thr}) below which very little atomization is observed, a transitional region over which aerosol generation is very sensitive to the atomizer voltage (steepness characterized by C_{V}, centered at V_{thr}), and a horizontal asymptote at higher voltages indicating a saturation in droplet generation at a maximum LDM value (LDM_{m}). Some aspects related to this type of data can be obtained by time-intensive printing studies, but the ability to collect this diagnostic of ink atomization without any post-processing or measurements following printing is empowering. For ink formulation, this characteristic could indicate whether an ink is able

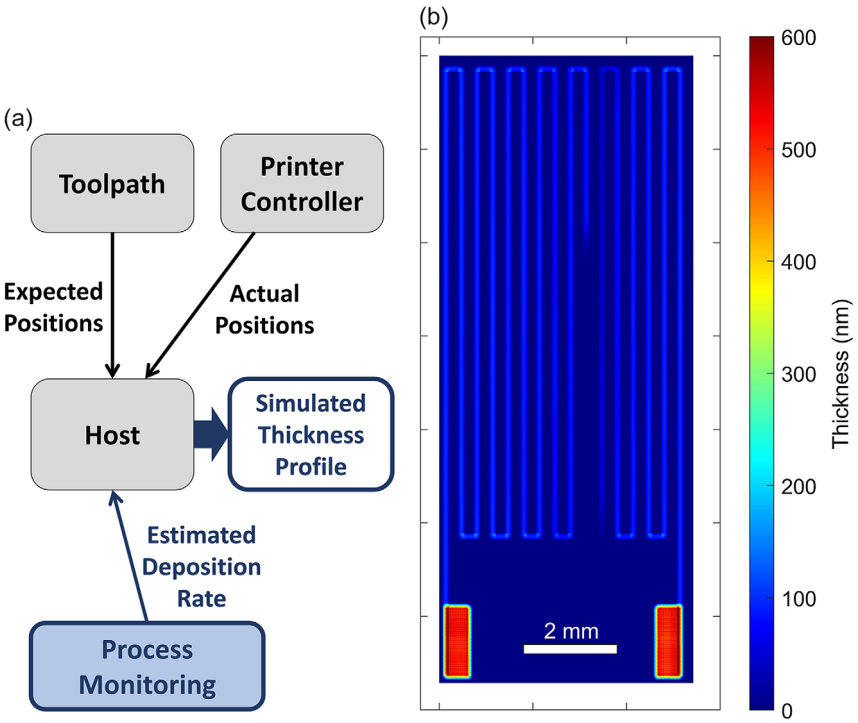

Figure 3. a) Diagram for print simulation capability, using calibration data to predict the profile based on measurements during the process. b) Demonstration of print simulation; in this case, a defect was introduced into the serpentine region, leading to a visible low spot in the predicted thickness.

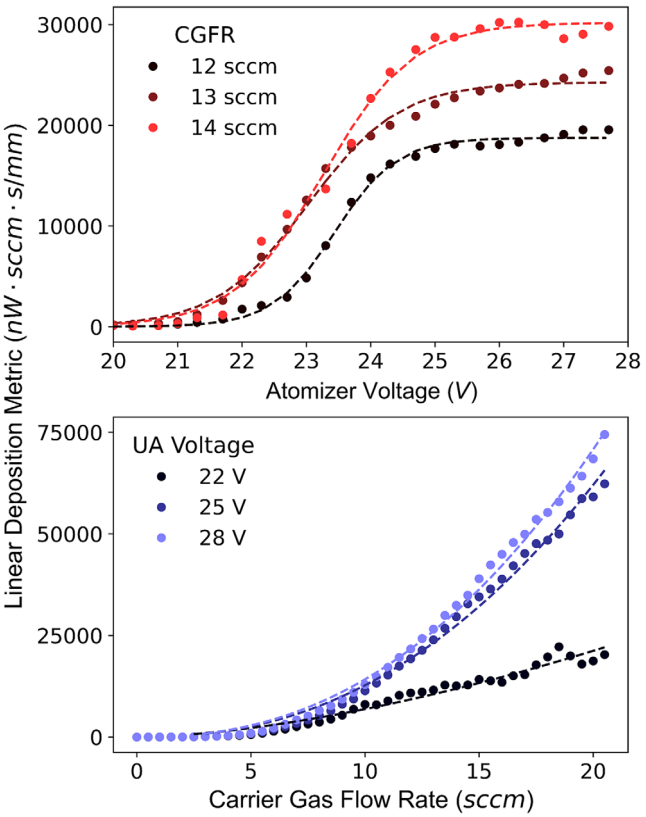

Figure 4. Response curves for a PMMA ink, showing the LDM dependence on (top) UA voltage setting and (bottom) CGFR. Adapted with permission.[24] Copyright 2023, Wiley.

to reach saturation within the constraints of the atomizer voltage and current, under what conditions the deposition is most sensitive to variations in atomization, and where the threshold in atomization occurs. Because this metric is independent of any downstream sheath-induced evaporation or impaction effects, it provides a very clean diagnostic for the ink itself, simplifying interpretation.

Notably, under the saturation conditions for atomization, the CGFR has a noticeable effect on determining the value of the LDM. This contribution is much higher than would be expected from the direct influence of the CGFR on LDM–a 17% increase in CGFR (from 12 to 14 sccm) corresponds to a ≈33% increase in the LDM, suggesting that approximately half of the increase is due to an increase in the scattering power. While there is little expected effect of CGFR on atomization directly in a UA system, the flow through transport channels to the printhead is anticipated to play a role.[27] This is the indirect effect observed in Figure 4, and this mechanistic clarity is unprecedented for AJP and can inform fundamental process studies.

This effect plays out in the response curve for the CGFR as well. For the sweep in CGFR, three different values of the atomizer voltage were evaluated—22, 25, and 28 V corresponding to near threshold, above threshold, and saturation. The CGFR was swept from 0 to 20 sccm for each. Importantly, this provides data that can be very challenging to get experimentally. In particular, at low deposition rates and very high focusing ratio, sheath-induced drying of the aerosol alters the impaction efficiency and dynamics; at very high deposition rates, liquid-phase spreading of the deposited ink leads to irregular line edges and complicates accurate measurements.[28] Those are not limitations for the in-line measurement, allowing a broader range of printing parameters to be evaluated to gain insight on the printing process.

As the CGFR is increased, the response curve in Figure 4 is fit well within this range using a power law expression with two fitting parameters, C_F and C_E, as

$$LDM = C_F * f_a^{C_E} \tag{6}$$

While the LDM has a direct linear relationship with CGFR, as shown in Equation (4), the observed superlinearity here is a manifestation of coupling effects, namely the transport efficiencies described earlier.[27] At very low CGFR, droplets sediment under gravity within the mist tube (or in the cartridge itself), leading to very low aerosol volume fraction in the optics cell. As the CGFR is increased, the transport efficiency becomes closer to 1, leading to more linear behavior at high CGFR. Some evidence of this may be apparent at high CGFR in Figure 4, but there remains insufficient data to evaluate whether this upper limit is indeed achieved within the range shown here. It appears most likely that it is achieved for the undersaturated condition (22 V). Importantly, the power law fit to this data is not a fundamental model, it is purely a reasonable empirical fit to this dataset. A more complex model describing this result could lead to improved fitting at both ends of the data set and capture the expected physics of linearity at high CGFR. Even so, this highlights the potential for increasing deposition rate with AJP by pushing to higher CGFR and higher print speed.

3.5. Fundamental Insight

By providing a physically relevant measurement between the cartridge and printer nozzle, the diagnostic capability of this process monitoring framework can support advanced analysis of the printing process itself. In particular, the use of the scattering measurement as an indicator of deposition rate is predicated on an assumption that material flowing through the optics cell will be deposited on the substrate. The linearity of the calibration curve (Figure 1c) is evidence that this is valid under many circumstances on a differential basis—i.e., that an additional increment of aerosol passing through the optical measurement cell will lead to a proportional amount deposited on the surface–but not on an absolute basis. Notably, if the assumption that droplets passing through the optics cell impact the surface with perfect efficiency, the y-intercept of the calibration curve would go to zero. The nonunity impaction efficiency that this measurement implies has been hinted at previously,[28] but the optical measurement upstream of the printhead offers much stronger experimental evidence.

We propose a methodology to extract fundamental information about the deposition process using this optical diagnostic. Two assumptions are necessary to support this analysis: first, that the droplet size remains within a narrow range, such that the differential scattering cross section does not significantly vary; and second, that at high deposition rates, where the calibration

curve (Figure 1c) is highly linear, the differential impaction efficiency is near unity. With these approximations, we can estimate mechanistically important process variables using a variation of the response curve experiment described in Figure 4. Here, a series of samples is printed with gradually increasing CGFR, and both the LDM and cross-section area of samples are measured (**Figure 5**a). At higher flow rates, both values increase fairly consistently, supporting the assumption that the differential impaction efficiency approaches unity (note that variability in the cross-section area at high CGFR reflects more irregular line profiles attributed to liquid-phase fluid migration). The interesting behavior occurs at lower CGFR, where these curves diverge. In particular, there is a range of samples for which droplets are passing through the optics cell, giving rise to a moderate LDM reading, but the accrual of material on the surface remains negligible. Using the second assumption from above, an estimate for the impaction efficiency can be calculated.

Specifically, Equation (3) describes proportionality between the deposition rate and the product of CGFR, scattering power, and impaction efficiency. Lumping the terms assumed constant with the proportionality factor, we get

$$r_{\text{dep}} = K(f_{\text{a}} P_{\text{sc}})\eta_i \tag{7}$$

The plot of r_{dep} vs. $f_{\text{a}}P_{\text{sc}}$ is shown in Figure 5b. At high deposition rates, a linear relationship is observed, which underscores the assumption that under these conditions the differential impaction efficiency is unity—that is, any incremental material passed through the nozzle will lead to a corresponding increment in deposited material, likely related to saturation of droplet evaporation effects. With this assumption, the proportionality constant K can be calculated as the slope in this linear region and then the impaction efficiency calculated directly from Equation (7).

This calculated impaction efficiency is plotted against the measured deposition rate in Figure 5c. Under the assumption that a fixed amount of material can travel through the nozzle with negligible impaction (i.e., evaporation limited),[28] this curve would follow $\eta_i = r_{\text{dep}}/(r_{\text{dep}} + C)$ with C a fitting constant. Indeed, the dashed line in Figure 5c is a curve fit to this basic model, yielding an r^2 value of 0.95 and supporting this simple conceptual approximation of the process mechanisms.

Finally, a quantitative value for the impaction efficiency allows the nominal aerosol volume fraction to be estimated using Equation (1). Figure 5d shows how this effective aerosol volume fraction changes as a function of the CGFR, exhibiting a monotonic increase. This is logically a reflection of transport losses

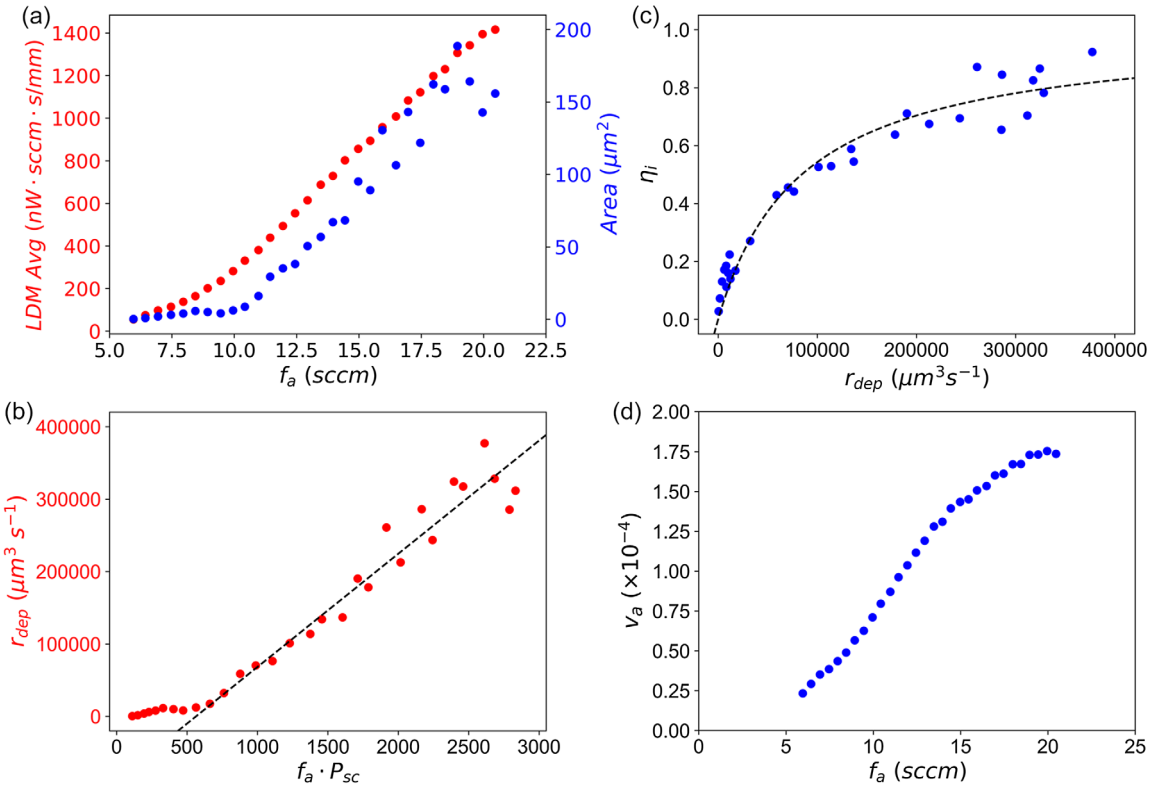

Figure 5. Diagnostic utility of in-line process monitoring to understand AJP mechanisms. a) Raw data from a flow rate sweep showing the disparity in material passing through the printhead (LDM) and that deposited on the surface (area) at low flow rates. b) Plot of the deposition rate as a function of the product of carrier gas flow and scattering power, showing a linear correlation after some threshold value is reached. c) Estimate of the impaction efficiency as a function of the deposition rate, showing a sharp drop to near-zero impaction efficiency at low deposition rates. This curve is effectively fit with a one-parameter model that assumes a constant nonimpacted volume. d) Estimate of the effective aerosol volume fraction as a function of the CGFR, showing a monotonic increase that reflects transport losses in moving droplets to the printhead.

within the printer, upstream of the printhead. This effect was speculated in prior work,[27] but no previous work known to the authors attempts to quantify or evaluate this effect in detail due to challenges in deconvoluting losses due to transport to the printhead and losses during the impaction stage. This combination of process monitoring hardware and experimental protocols thus offers an unprecedented capability to better understand the process science of AJP and leverage that understanding for improved performance and control.

3.6. Outlook and Limitations

The process monitoring technology discussed here has broad value in AJP, across both R&D and production. It provides a diagnostic of the aerosol state within the printhead, which can help deconvolute different failure modes during ink and process development. Moreover, its potential for closed-loop control to reduce process drift over long production runs addresses a key challenge for AJP. In addition, the spatial correlation of this real-time metric within a print can inform quality control frameworks, a key consideration for serial production across additive manufacturing methods. The general utility of this stems from its physical significance, starting with its development centered around an understanding of leading contributors to drift and variability in AJP. Its demonstration for a range of inks, including the AgNP and PMMA shown here, along with magnetite NPs and graphene in previous work,[22,23] validates the strength of Mie scattering for aerosol droplets of sizes relevant to AJP for the broad range of optical properties represented by these different ink. The extension of this method to PA remains to be done, but the mechanistic basis for the method suggests a straightforward extension. In particular, this method relies on strong scattering from aerosol droplets in the ≈0.5–5.0 μm size range, which is applicable to PA systems for AJP. The higher volume fraction of droplets will increase the scattering signal, potentially altering the optimal optics configuration. In extreme cases, this could alter the linearity of the deposition rate-scattering relationship, but this is not a prerequisite to process monitoring and control, only a convenience that simplifies interpretation. The development of closed-loop control strategies for PA will be more involved, particularly given the challenge with secondary effects observed with CGFR modulation for the UA system.[24] While our capabilities to date have not allowed experimental validation of this system for PA, this remains a strong focus of future work. In addition, the consistency and calibration of this system day-to-day and machine-to-machine remains an open question and will influence its convenience and thus adoption.

While it is tempting to reduce variability to a single metric–captured by the aerosol volume fraction or scattering power–this remains an imperfect approximation. Accuracy is only expected within a narrow scope of processing space, and changes to ink composition, cartridge loading, atomization, and flow conditions could cause deviations. Changes to the droplet size distribution, in particular, are a difficult source of potential deviation because limited means exist by which to address them. The droplet size distribution is a key contributor to the correlation between scattering power and aerosol volume fraction, and sources of variability that affect the volume fraction would also likely influence the droplet size distribution. The stability and linearity of the correlation as shown here are promising evidence that, within a narrow window of process space, size variations are limited or have limited effect on this correlation. However, a more quantitative effort to estimate and cap deviation caused by variation in droplet size would improve confidence in this method, particularly when applied to closed loop control. In addition, orthogonal sensing modalities that are sensitive to droplet size characteristics could provide a valuable source of information to complement the single scattering power reading, and recent efforts to advance these by LaRiviere, et al. have demonstrated technical feasibility.[30]

Although the sensitivity of the scattering-deposition rate correlation to droplet size and composition limits extensibility during closed-loop control, this same characteristic supports more thorough evaluation of variability sources in the process. In this capacity, it offers value in scientific studies to move the field forward with a bottom-up understanding of process mechanisms. Alongside its utility for ink and process development, this represents a key area this technology is being applied distinct from the engineering-driven efforts in closed-loop control and process simulation.

4. Conclusion

The AJP process monitoring technology based on light scattering from the aerosol stream begins to offer a glimpse of the system state within the printhead. With its close relation to the aerosol volume fraction, this measurement provides a valuable diagnostic that can bridge fundamental process understanding with empirical printing outcomes, offering a viable technique to improve fabrication reliability and accelerate ink and process development. Progress in this technology to date has been driven by improved understanding of basic AJP mechanisms, motivating further efforts to understand first what should be measured. Ultimately, this will offer a promising method to improve digital integration of AJP, offering a handle to build automation in both factory and laboratory environments.

5. Experimental Section

Materials: Several different inks have been used to validate the process monitoring system. The results presented here corresponded to a PMMA ink (Figure 4 and 5) and AgNP ink (Figure 1–3). The PMMA ink was a dilute solution (10 mg mL^{-1}) of poly(methylmethacrylate) (≈15 000 M_w, Acros Organics) in a solvent mixture of 9:1 v v^{-1} xylenes (Acros Organics)/terpineol (Millipore-Sigma). The AgNP ink was based on a commercial silver nanoparticle dispersion (Ag40X, UTDots) in xylenes; the printed ink contained 2:7:1 stock Ag40X/xylenes/terpineol.

Printing: All printing experiments were carried out on a custom AJP system, using compressed air for the carrier and sheath gas, ultrasonic atomizers for aerosol generation, and a heated print bed mounted on an x-y motion system for patterning. Unless otherwise noted, data corresponded to a tapered nozzle with a diameter of 200 μm. The light source used for experiments shown here was a 30 mW, 940 nm laser diode from Thorlabs.

Characterization: Following deposition and curing of the inks, optical microscopy was performed with a Motic microscope. Line cross-section profiles were collected using a Keyence displacement sensor mounted on the printing system or with a Zygo NewView 9000 optical profilometer.

Electrical measurements were collected using an electrical probe station with a 4 pt measurement configuration using a Keithley 2400 Series source-measure unit.

Software Tools: The AJP system was controlled via a custom Python program and associated modules. To implement the capabilities discussed here, a module was created to integrate the light scattering measurement with the software controller.

Acknowledgements

The authors acknowledge funding to support this work provided by the National Science Foundation under grant NSF CMMI-2224303.

Open access funding provided by the Iowa State University Library.

Conflict of Interest

The authors declare no conflict of interest.

Keywords

additive manufacturing, hybrid electronics, printed electronics, process control, process monitoring

Received: August 25, 2023
Revised: October 27, 2023
Published online: November 10, 2023

[1] D. R. Hines, Y. Gu, A. A. Martin, P. Li, J. Fleischer, A. Clough-Paez, G. Stackhouse, A. Dasgupta, S. Das, *Addit. Manuf.* **2021**, *47*, 102325.
[2] J. Q. Feng, M. J. Renn, *J. Micro Nano-Manuf.* **2019**, *7*, 011004.
[3] J. A. Paulsen, M. Renn, K. Christenson, R. Plourde, in *2012 Future of Instrumentation Inter. Workshop (FIIW) Proc.*, Gatlinburg, TN, USA, 8–9 October **2012**, pp. 1–4.
[4] M. T. Craton, X. Konstantinou, J. D. Albrecht, P. Chahal, J. Papapolymerou, *IEEE Trans. Microw. Theory Techn.* **2020**, *68*, 3418.
[5] Y. Piro, C. Areias, A. Luce, M. Michael, P. Biswas, O. Ranasingha, J. F. Reuther, S. Trulli, A. Akyurtlu, *ACS Appl. Mater. Interfaces* **2023**, *15*, 35449.
[6] E. S. Rosker, M. T. Barako, E. Nguyen, D. DiMarzio, K. Kisslinger, D.-W. Duan, R. Sandhu, M. S. Goorsky, J. Tice, *ACS Appl. Mater. Interfaces* **2020**, *12*, acsami.0c06959.
[7] Y. Gu, D. R. Hines, V. Yun, M. Antoniak, S. Das, *Adv. Mater. Technol.* **2017**, *2*, 1700178.
[8] N. X. Williams, N. Watson, D. Y. Joh, A. Chilkoti, A. D. Franklin, *Biofabrication* **2020**, *12*, 025004.
[9] E. W. C. Phuah, W. L. Hart, H. Sumer, P. R. Stoddart, *Bioprinting* **2020**, *18*, e00081.
[10] Y. Gu, D. Park, D. Bowen, S. Das, D. R. Hines, *Adv. Mater. Technol.* **2019**, *4*, 1800312.
[11] S. Vella, C. S. Smithson, K. Halfyard, E. Shen, M. Chrétien, *Flex. Print. Electron.* **2019**, *4*, 045005.
[12] X. Chen, J. M. Lawrence, L. T. Wey, L. Schertel, Q. Jing, S. Vignolini, C. J. Howe, S. Kar-Narayan, J. Z. Zhang, *Nat. Mater.* **2022**, *21*, 811.
[13] Md. A. Ali, C. Hu, S. Jahan, B. Yuan, M. S. Saleh, E. Ju, S. Gao, R. Panat, *Adv. Mater.* **2021**, *33*, 2006647.
[14] N. Kempf, Y. Zhang, *Rev. Sci. Instrum.* **2021**, *92*, 105008.
[15] B. A. Lariviere, P. C. Joshi, T. J. Mcintyre, *IEEE Access* **2020**, *8*, 211085.
[16] M. Smith, Y. S. Choi, C. Boughey, S. Kar-Narayan, *Flex. Print. Electron.* **2017**, *2*, 015004.
[17] R. R. Tafoya, E. B. Secor, *Flex. Print. Electron.* **2020**, *5*, 015009.
[18] R. (Ross) Salary, J. P. Lombardi, P. K. Rao, M. D. Poliks, *J. Manuf. Sci. E.-T. ASME* **2017**, *139*, 101010.
[19] J. P. Lombardi, R. (Ross) Salary, D. L. Weerawarne, P. K. Rao, M. D. Poliks, *J. Manuf. Sci. Eng.* **2019**, *141*, 071011.
[20] R. (Ross) Salary, J. P. Lombardi, D. L. Weerawarne, M. S. Tootooni, P. K. Rao, M. D. Poliks, *J. Manuf. Sci. Eng.* **2020**, *142*, 081007.
[21] Y. Gu, D. Gutierrez, S. Das, D. R. Hines, *J. Micromech. Microeng.* **2017**, *27*, 097001.
[22] R. R. Tafoya, A. W. Cook, B. Kaehr, J. R. Downing, M. C. Hersam, E. B. Secor, *Adv. Mater. Technol.* **2020**, *5*, 2000781.
[23] E. B. Secor, *Addit. Manuf.* **2021**, *44*, 102028.
[24] J. D. Rurup, E. B. Secor, *Adv. Eng. Mater.* **2023**, *25*, 2201919.
[25] A. Wadhwa, Run-Time Ink Stability in Pneumatic Aerosol Jet Printing Using a Split Stream Solvent Add Back System, **2015**.
[26] P. Lall, A. Abrol, N. Kothari, B. Leever, S. Miller, *J. Electron. Packag.* **2020**, *142*, 041003.
[27] E. B. Secor, *Flex. Print. Electron.* **2018**, *3*, 035002.
[28] E. B. Secor, *Flex. Print. Electron.* **2018**, *3*, 035007.
[29] R. R. Tafoya, E. B. Secor, *Flex. Print. Electron.* **2020**, *5*, 035004.
[30] B. A. LaRiviere, P. W. Groth, P. C. Joshi, M. N. Ericson, *IEEE Access* **2023**, *11*, 99159.

Jeremy D. Rurup is a graduate research assistant in the Department of Mechanical Engineering at Iowa State University. Currently, his research is centered around aerosol jet printing with a focus on fundamental process science and in situ process monitoring, with forthcoming work in conformal electronics printing and structural electronics.

Ethan B. Secor is an Assistant Professor in the Department of Mechanical Engineering at Iowa State University. His research interests include printed electronics, nanomaterial inks, aerosol-based deposition methods, and advanced manufacturing, with a current emphasis in aerosol jet printing spanning fundamental mechanisms, ink formulation, process monitoring and control, and multimaterial patterning.